Constructing a deformable human hand model in contact for virtual ergonomic assessment

Yulai XIE[1], Satoshi KANAI[1] and Hiroaki DATA[1]
[1] Graduate School of Information Science and Technology, Hokkaido University, Japan,
y_xie@sdm.ssi.ist.hokudai.ac.jp, {kanai, hdate}@ssi.ist.hokudai.ac.jp

Abstract:
Skin contact deformation plays a significant role in the virtual ergonomic assessment of handheld products. In this paper, a physical model with nonlinear elasticity and compressing-swelling effect of skin is proposed. Based on the model, we present an efficient contact solving method to simulate physical contact with product surfaces. According to the knowledge of hand surface anatomy, the hand surface skin is partitioned into different regions for being able to specify different physical parameters and for efficient simulation. The realistic contact deformations not only of fingers and a palm in simple contact conditions, but also in more practical grasp postures, were efficiently realized and experimentally verified. The verification results showed that the proposed deformable hand model could effectively approximate contact area, contact force and contact pressure distribution in an acceptable range for virtual ergonomic assessment.

Keywords: Virtual Ergonomic Assessment, Digital Hand, Skin Contact Deformation, Nonlinear Elasticity, Compressing-swelling effect

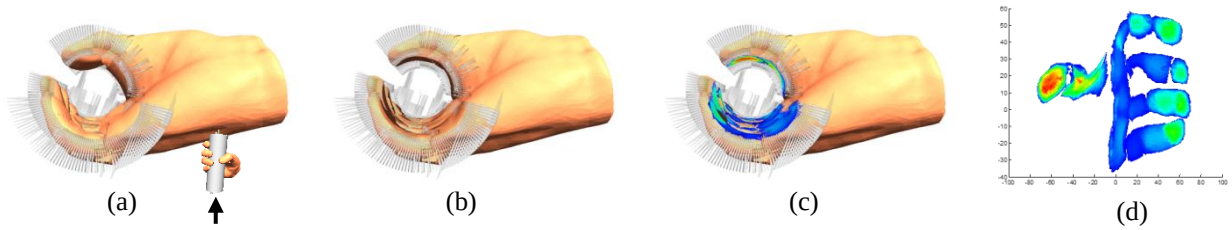

Figure.1 Simulation of grasp posture griping a ϕ48mm cylinder. (a) Skin before deformation, (b) Skin after deformation, (c) Pressure distribution map, (d) Extended 2D pressure distribution map

1. Introduction

1.1 Background

Ergonomic-conscious design of handheld products, such as digital handheld appliances, handy tools and containers, brings a better user experience to customers, and contributes to strengthening their market competitiveness. However, conventional ergonomic assessment of these products, such as comfort or fatigue estimation, still greatly depends on sensory tests by real human subjects. Moreover, the preparation of expensive physical mockups and questionnaire-like user surveys are high in cost and time consuming, and only the subjective and qualitative evaluation results can be obtained.

On the other hand, since fierce market competition requires manufactures to shorten product development cycles, reduce costs and improve efficiency, virtual ergonomic assessment technique has rapidly been developed. Virtual ergonomic assessment benefits the manufactures to fulfill the requirements mentioned above, and also enables quantitative evaluations. However, so far, no commercially available virtual ergonomic assessment tool for handheld products has been made available.

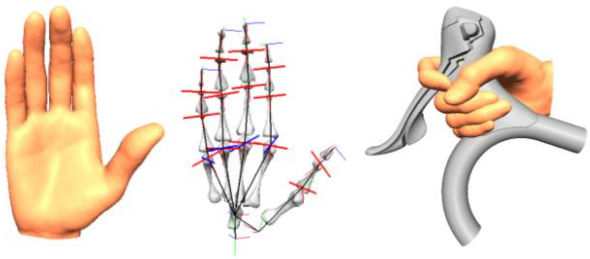

Figure.2 Digital Hand. (a) Skin surface mesh, (b)Internal bone meshes, (c) Grasp posture generation

To solve this problem, our research group have been proposing the Digital Hand [1, 2] (Fig.2), a virtual hand model and virtual ergonomic assessment system for handheld products. The Digital Hand is represented by a 3D skin surface mesh (Fig.2 (a)) and 3D internal bone meshes (Fig.2 (b)) derived from MRI measurements of human hands [2]. The finger and palm motion of humans, and skin deformation caused by motion are precisely simulated. Moreover, the Digital Hand enables us to generate plausible grasp postures (Fig.2 (c)) and also predict the quantitative measures of grasp such as grasp quality and grasp fitness [1].

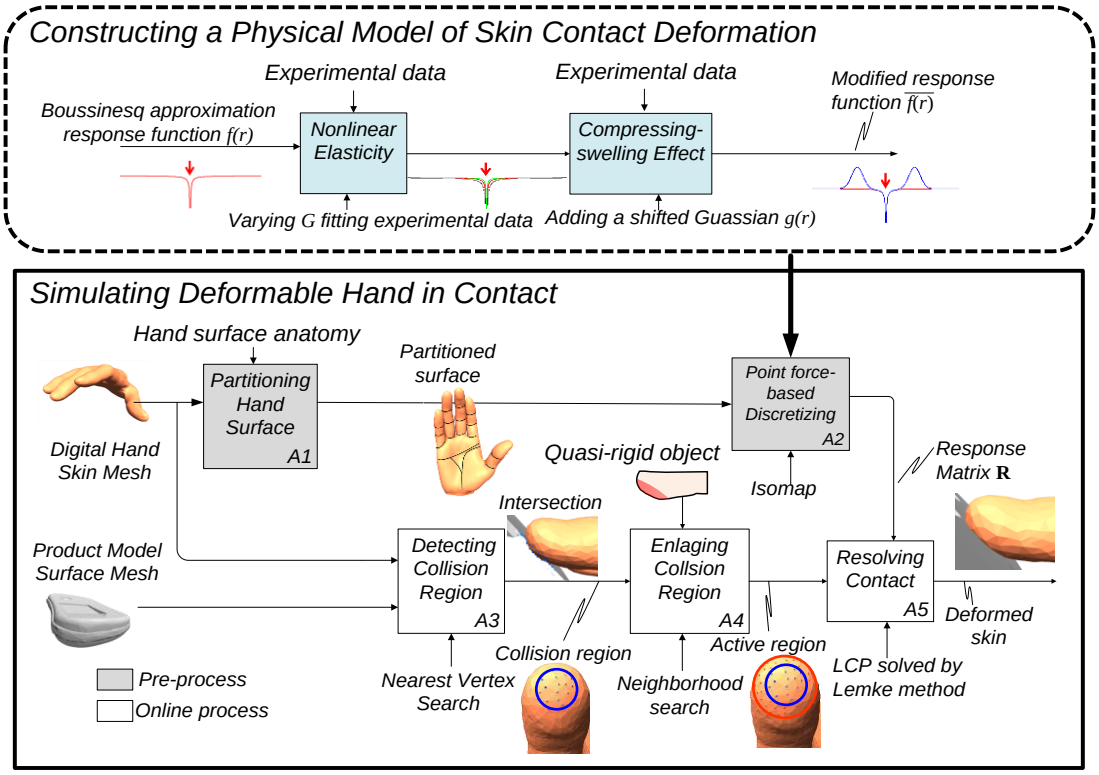

Figure.3 Our proposed system of deformable human hand model in contact

1.2 Purpose

The biomechanical property of hand skin has been known to play a fundamental role [3, 4] in the tactile sense of humans. The direct contact between hand skin and objects results in contact force, contact area, and contact pressure distribution. Especially, pressure distribution is essential in the evaluation of grasp stability, comfort and safety. For instance, a poor design of hand tools may result in cumulative trauma disorders due to high local contact pressure [5].

At present, manufacturers of handheld products can get some indices about these contact conditions in simple grasps from experiments, e.g. grip strengths and pressure distributions, using measurement devices, e.g. Jarmar dynamometers, force gauges and data-gloves with pressure-sensitive materials.

As for virtual ergonomic assessment of grasp, skin deformation in contact is also desired. However, the current Digital Hand does not simulate hand skin deformation caused by physical contact with product surfaces, and instead approximates it in a simple way where the interpenetration between the skin and the surfaces within a specific threshold is allowed [1].

The requirements on the simulation of skin contact deformation for a practical virtual ergonomic assessment based on the Digital Hand are as follows:

1) **Sufficient accuracy**: Excessive precision is not pursued, but some important contact conditions such as contact force, contact area, the pressure distribution and the high pressure area should be as same as the experimental ones to an acceptable extent. Hence, two important properties, nonlinear elasticity and compressing-swelling effect, should be realized for the accuracy in the simulation.

2) **Higher efficiency**: In a practical virtual ergonomic assessment process, a large number of grasp postures with different hand sizes need to be generated within a short period of design, and the simulation of skin contact deformation also needs to be repeated at the same time. So the simulation method should have a computational performance as fast as possible, and does not burden the designers with time-consuming simulation.

3) **Compatibility with the existing Digital Hand**: The existing Digital Hand has a grasp posture generation algorithm and grasp assessment functions. Since its skin surface is modeled as a triangular mesh, we must ignore the layer structure of skin. The material property presented by surface skin is used to represent that of the entire skin. And we deal with displacements and forces at the vertices and areas over the triangles in the deformation simulation.

Therefore, the purpose of this paper was to construct a deformable human hand model in contact for virtual ergonomic assessment. To achieve this goal, we made the following contributions: 1) a nonlinear elasticity model of hand skin deformation is proposed, 2) the property of compressing-swelling effect of hand skin deformation is measured and reflected to the deformation model, 3) a partition of hand surface is proposed for accuracy and efficiency, 4) an efficient contact solving method is introduced, and 5) efficient skin deformation simulation of grasping postures is realized. And the estimated contact conditions, such as contact force, contact area, and contact pressure distribution, was also experimentally verified.

1.3 Overview

As shown in Fig.3, constructing our deformable human hand model in contact is composed of two main parts: 1) constructing a physical model of skin contact deformation, and 2) simulating a deformable hand in contact.

In the first part, a physical model of skin contact deformation based on Boussinesq approximation is introduced, and nonlinear elasticity and compressing-swelling effect are extended for mimicking realistic behavior of skin contact deformation. In the second part, based on the proposed physical model, an algorithm to simulate a deformable hand is developed. The algorithm includes a pre-process and an online process. In the pre-process, the hand surface of the Digital Hand is partitioned based on hand surface anatomical knowledge for accuracy and efficiency (A1). Then, we introduce the point-force-based discretization of the physical model in order to calculate response matrices between vertices in each partitioned surface (A2). For one Digital Hand, this pre-process has to be executed only once. While in the online process, a collision detection algorithm is used to find collision regions between the Digital Hand and the product model surface (A3). Then, under the concept of a quasi-rigid object, collision regions are locally enlarged to get active regions (A4). Finally, based on the calculated response matrices, the contact deformations over the active regions are simulated by solving the Linear Complementarity Problem (LCP) (A5).

In the following sections of this paper, Section 2 introduces the related works. Section 3 and 4 describe our physical model and the algorithm of simulating deformable hand in contact. Section 5 presents the simulation results and corresponding experimental verifications. Conclusions are given in Section 6.

2. Related Works

2.1 Grasp evaluation s in Conventional Ergonomics

There have been several experimental studies on handheld product contact behaviors in the conventional ergonomics field.

Aldien et al. [6] used three different cylindrical handles to measure the hand-induced forces and distributed pressure using a capacitive pressure-sensing mat wrapped around the handle. They found that distribution of localized pressure peaks and the resulting contact force over the hand surface were associated with discomfort and pain in the hand. Seo et al. [7] also summarized different grip force measurement methods.

However, these evaluations basically had the problems of inefficiency and high cost.

2.2 Hand modeling and Grasp Synthesis

In CG studies, ElKoura et al. [8] had proposed a data driven algorithm for modeling the sympathetic motion between fingers of the hand for playing musical instruments. Sueda et al. [9] described an automatic technique for generating the motion of tendons and muscles of a hand in an animated character. Rhee et al. [10] utilized the contours and surface anatomical creases visible in photographs of individual's hand to make a person-specific hand model. Liu et al. [11] introduced an optimization-based approach to synthesizing hand manipulations from a starting grasping pose. Miyata et al. [12] developed an algorithm which can generate realistic grasp postures for cylinders based on real finger postures from motion capture data.

Some of them realized finger bending deformations, but none of them realized plausible hand skin contact deformations with products.

2.3 Skin Contact deformation simulation

FEM-based methods have been used to simulate finger contact deformation [3, 13] with higher accuracy. Bickel et al. [14] also presented a combined approach of data-driven and linear FEM-based contact deformation for representing nonlinear heterogeneous soft tissue. Tao et al. [15] partitioned hand surface, and then built an FEM model for stress analysis in contact to estimate hand pressure distribution for handle grasps. However, the simulation efficiency was not clearly discussed in them. Although [14] seems to be fast, it did not state the elapsed time. Also, their method was not proven proper for skin deformation in grasp postures. The other FEM-based methods are not suitable for practical virtual ergonomic assessments due to the low efficiency and coverage.

On the other hand, in CG, Pauly et al. [16] did a pioneering work for efficient simulation contact deformation, but the physical meaning of human hand skin was not taken into account. Also, the experimental verification was insufficient. Jain et al. [17] developed a practical system to simulate two-way coupling between rigid and deformable bodies in a robust and efficient manner. They demonstrated that the simulation of soft tissue deformation at the site of contact could achieve very robust and realistic motion. However, similarly, the biomechanical parameters were chosen without any evidence and did not resemble human skin or muscle materials in the real world.

[16] is an important reference in our paper, but we made significant improvements and the necessary simplification for practical virtual ergonomic assessment. The differences between [16] and our research are summarized as follows (the former is the feature of [16], and the latter is ours):

1) Elasticity: Linear Boussinesq approximation vs. nonlinear Boussinesq approximation.
2) Compressing-swelling effect: Simulated by adding a Guassian function vs. simulated by adding a shifted Gaussian.
3) Homogeneity of the physical property: Homogenous vs. heterogeneous.
4) Basic geometric model: Point-based model vs. irregular triangle mesh model.
5) Force representation: Pressure distribution vs. point forces at vertices.

6) Experimental verification: Insufficient vs. sufficient.

3. Physical Model of Skin Contact Deformation

3.1 Boussinesq Approximation

Boussinesq approximation, a widely used method in contact mechanics, models linear elasticity with a constant shear modulus in small deformation. It approximates the surface deformation around a contact point with an elastic half space [18]. The displacement-force relation is expressed by Eq.1, and the curve shown in Fig.4.

$$u(r)=\frac{(1-\upsilon)p}{2G\pi r}=f(r)p, \qquad f(r)=\frac{(1-\upsilon)}{2G\pi r} \tag{1}$$

where, as shown in Fig.4, r is the distance between a point and the origin, $u(r)$ is the displacement at a point away from the origin by r due to a normal concentrated force, p, acting at the origin, υ Possion's ratio, G shear modulus, and $f(r)$ response function.

3.2 Nonlinear Elasticity of Skin

Human skin has a complicated biological structure and presents nonlinear elasticity in the stress-strain relationship [3, 4, 19], i.e., Young's modulus varies with strain, owing to the different structures of the elastin and the collagen fibers which are the main components of dermis in different stressing or straightening states.

For ergonomic assessment, we mainly considered the external geometry of a hand, and therefore hand skin can be treated as a bulk material [20]. This means that the layer structure of skin is ignored, and the physical property presented by surface skin is used to represent that of the entire skin. From in-vivo experiments, the average Possion's ratio υ of the human skin varies from 0.45 to 0.50 [21]. As in our simulation human skin is regarded as a quasi-incompressible material, 0.5 was chosen for υ based on [21].

As for Young's modulus, unfortunately, the values of soft tissue can vary by a factor of 3000, depending on the model proposed and the measurement techniques, ranging from 0.02 MPa to 57 MPa [22]. While [3] showed that the shear modulus G of human hand skin ranges from 0.004MPa to 0.08MPa, which was measured by an indentor test of human fingers in-vivo in small deformation (1mm). We use this range of G as a reference of our physical model with nonlinear elasticity. Nonetheless, setting material parameters of hand skin is still a difficult and time-consuming process. Considering the nonlinearity, the process becomes more challenging. Therefore, in order to realize nonlinear elasticity, we tuned shear modulus G to fit our real experimental data obtained from subjects to find the right range of G based on the experiment in Section 5.1.

3.3 Compressing-swelling Effect

As human skin is a quasi-incompressible material [20], in our skin deformation simulation, the compressing-swelling effect needs to be realized. This means that compressive force causes not only regional volume compression in the force acting region, but also regional volume swelling right outside the region due to

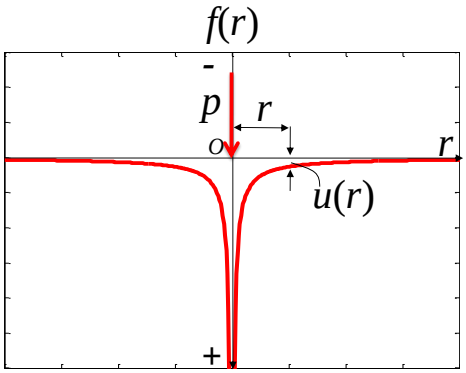

Figure.4 Response function of Boussinesq approximation

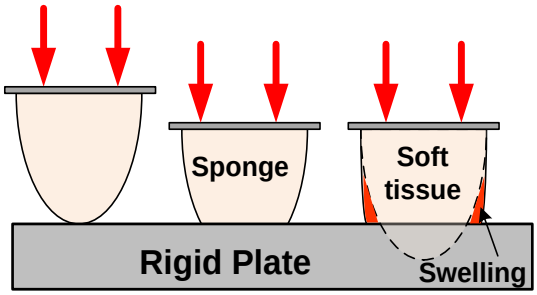

(a) (b) (c)

Figure.5 Compressing-swelling effect. (a) Reference, (b)Sponge (compressible material without compressing -swelling effect), (c) Soft tissue (incompressible material with compressing-swelling effect)

a finite volume. However, as shown in Fig.5(b) the volume after deformation is obviously reduced when using the original Boussinesq approximation, and it leads to the behaviors of a sponge-like material. The compressing-swelling effect of an incompressible material, such as a soft tissue like that shown in Fig.5(c), is needed in our skin deformation simulation to cause more realistic deformation and give a relevant contact area.

3.4 Nonlinear Elasticity Model Based on Modified Boussinesq Approximation

In order to realize nonlinear elasticity in our physical model, shear modulus G is regarded as a function of a penetration depth, d, as Eq.2:

$$G(d)=G(d)+\frac{d}{d_{\lim}}(G_{\max}-G_0) \tag{2}$$

where G_0 is an initial shear modulus, $G_{\max}$ a maximum shear modulus, and $d_{\lim}$ a limit penetration depth. In this way, with increasing of penetration depth, hand skin becomes more rigid.

On the other hand, to realize the compressing-swelling effect, we modulated the original Boussinesq approximation, as shown as the blue thick curve in Fig.6, by adding a shifted Gaussian function (the red curve) in the opposite direction, as Eq.3:

$$\overline{f(r)} = f(r) - g(r) = f(r) + \left\{ -a \exp\left(\frac{-(r-b)^2}{2c^2} \right) \right\} \quad (3)$$

where $\overline{f(r)}$ is the modified response function and $g(r)$ the shifted Gaussian function. In order to realize realistic swelling effect, we tuned a, b and c to fit our real experimental data obtained from subjects to find the right range of G based on the experiment in Section 5.1

4. Simulating Deformable Hand in Contact

4.1. Partitioning Hand Surface

The palmar side of a hand surface is the main contact area of our grasp. The surface anatomy of the main creases on the palm is a common landmark in hand surgery, since the basic main creases have a strong relationship with the underlying bone structure [10].

In the Digital Hand, the movements of the internal bone meshes under the skin surface mesh such as bending fingers and closing the hand, will cause the skin deformation, which is consistent with the real joint motion of humans. Therefore, the surface anatomy by main creases was used as the partition of palmar hand surface, as shown in Fig.7. The center of the palm (region #17) formed a less potential contact region in hand closing, so it was defined as an independent region. Although region #18 is in the dorsal side of the hand, it is treated as a potential contact region during grasping in our model.

The different areas on the palm have different sensitivity to externally applied surface pressure [5], which is related to the arrangement of nerves and blood vessels, and the underlying bones and muscles. These regions, divided by main creases, exhibit independent contact deformation behavior during hand motion. Therefore, we can specify the different shear modulus G in the different palmar regions. Moreover, the deformation simulation involving the entire hand surface mesh is inefficient. So the partition enables us to evaluate small response matrices in the small regions instead of calculating a large size response matrix of the entire hand surface mesh.

4.2 Point-force-based Discretizing

In the Digital Hand, the hand skin surface is presented by an irregular triangular mesh, which results in an uneven problem of force effect. This means that some forces which have larger neighboring regions will exert a larger effect than those with the same force magnitude but smaller neighboring regions. Therefore, to weaken such irregularities, we assumed that pressure distribution on triangles can be replaced by point forces

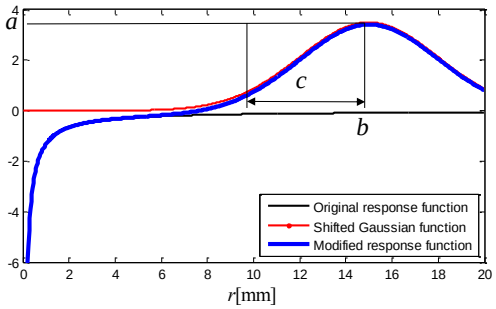

Figure.6 Our modified response function

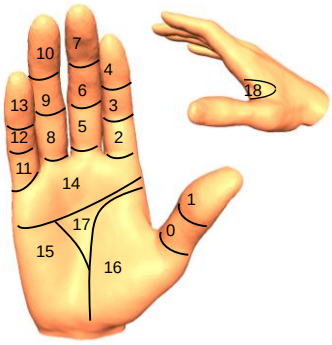

Figure.7 Partition of hand surface

concentratedly acting at vertices. Consequently, normal concentrated force p in Eq.1 can be considered as a constant, and the time-consuming numerical integration for a specific pressure distribution can be avoided. For a skin surface triangular mesh, the distance r in Eq.1 needed to be a geodesic distance between two vertices. Therefore, Isometric Mapping (Isomap) [23] which projects 3D vertices to a 2D plane and preserves geodesic distance was applied to reduce the 3D geodesic distance evaluation to the 2D Euclidean distance evaluation.

Moreover, in the discretization setting, we needed to find the relations between a force p_i acting on a vertex $\boldsymbol{q}_i$, and the displacement u_j that the vertex $\boldsymbol{q}_j$ experiences. The response relation R_{ij} can be expressed in the matrix form in Eq.4:

$$\mathbf{u} = \mathbf{R}(d_{\max})\mathbf{p} \quad (4)$$

where

$R(\mathrm{d_{max}}) = \left[\mathrm{R}_{ij}(\mathrm{d_{max}}) \right]$: system reponse matrix,

$$\mathrm{R}_{ij}(\mathrm{d_{max}}) = \frac{1}{\mathrm{G}(\mathrm{d_{max}})} \mathrm{R}_{\mathrm{ij}}^{\mathrm{Bou}} + \left(-\mathrm{a}(\mathrm{d_{max}})\ \mathrm{R}_{\mathrm{ij}}^{\mathrm{Gau}} \right),$$

$R^{\mathrm{Bou}} = \left[\mathrm{R}_{\mathrm{ij}}^{\mathrm{Bou}} \right]$: Boussinesq response matrix,

$$\mathrm{R}_{\mathrm{ij}}^{\mathrm{Bou}} = \frac{(1-\upsilon)}{2\pi\, \mathrm{r}_{\mathrm{ij}}},$$

$R^{\mathrm{Gau}} = \left[\mathrm{R}_{\mathrm{ij}}^{\mathrm{Gau}} \right]$: shifted Gaussian response matrix,

$$\mathrm{R}_{\mathrm{ij}}^{\mathrm{Gau}} = \exp\left(\frac{-(\mathrm{r}_{\mathrm{ij}} - \mathrm{b})^2}{2\mathrm{c}^2} \right),$$

$\mathbf{u} = [u_1, \ldots, u_N]^T$ is a vector of the displacements, N the number of vertices in an active region, $\mathbf{p} = [p_1, \ldots, p_N]^T$ a corresponding normal force vector, r_{ij} the geodesic distance between $\mathbf{q}_i$ and $\mathbf{q}_j$, $d_{\max}$ the maximum penetration depth among the vertices included in the active region. And if $\mathbf{q}_j$ is in the force acting region (Section4.4), $a(d_{\max}) = 0$.

For one Digital Hand model, we can pre-compute all the entries of $\mathbf{R}^{Bou}$ and $\mathbf{R}^{Gau}$ in the pre-process, which enables a relatively fast execution speed in the following online process.

4.3 Detecting and Enlarging Collision Region

Practical deformation simulation involving all of the vertices lacks efficiency; hence we modeled the human hand as a quasi-rigid object. *Quasi-rigid* [16] indicates as shown in Fig.8 that, when the objects' surfaces undergo small deformation within the vicinity of force acting regions, called the *active region*, the remaining shape of the objects still holds. In fact, hand tissue that appears rigid visually is actually deformable and can be modeled in this way. When the Digital Hand contacts a product surface, an interpenetration region between them (called a *collision region*) can be detected. The deformation is only allowed in the collision region and its local neighboring region as an active region. This local deformation in the active region enables faster simulation. An active region sometimes goes beyond the bounding of the partition in Fig.7.

We used a collision detection algorithm proposed in [1]. Once a collision region is found, by a neighborhood query based on the mesh model, the active region can be obtained. In our simulation, the union of the collision regions and its local neighboring vertices was used as an active region. To cover the convex portion of the response function in Fig.6, which corresponds to the bulges, 5 ring neighboring vertices were used as the local neighboring region for fingers, and 8 ring neighboring vertices for the palm in our model.

4.4 Resolving contact using LCP

The goal of this step is to realize the deformed surfaces caused by contact without interpenetration. In active regions, as shown in Fig.9 (a), we define s_i, the states of the vertex $\mathbf{q}_i$. $s_i > 0$ indicates the *separation* state, $s_i = 0$ the *contact* state, $s_i < 0$, the *collision* state. p_i is the normal force acting on $\mathbf{q}_i$. d_i is the signed distance between $\mathbf{q}_i$ and its nearest triangle face on product surface mesh. In Fig.9 (b), we observe that the state s_i and the force p_i are complementary at each vertex. To be able to have a non-zero force ($p_i > 0$), we must have a zero state ($s_i = 0$, the *contact* state), and to have a non-zero state ($s_i > 0$, the *separation* state) we must have a zero force ($p_i = 0$).

Therefore, we can combine these complementarity conditions to obtain,

$$\mathbf{s}=\mathbf{R}(d_{\max})\mathbf{p}+\mathbf{d}, \quad \mathbf{s}\geq 0, \quad \mathbf{p}\geq 0, \quad \mathbf{s}^T\mathbf{p}=0 \qquad (6)$$

where $\mathbf{s} = [s_1, \ldots, s_N]^T$: a state vector indicating the contact state, $\mathbf{R}(d_{\max})$ is a response matrix, $\mathbf{d} = [d_1, \ldots, d_N]^T$: a vector of the penetration depth at each vertex in the active region, $d_{\max} = \max(\mathbf{d})$, $\mathbf{p} = [p_1, \ldots, p_N]^T$: a vector of the force at each vertex in the active region. This is a linear complementarity problem (LCP). A solution of LCP can be found by Lemke's method [24].

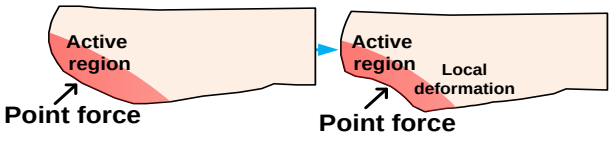

(a) (b)

Figure.8 Quasi-rigid object. (a)A point force is applied, (b)Local deformation is formed in active area

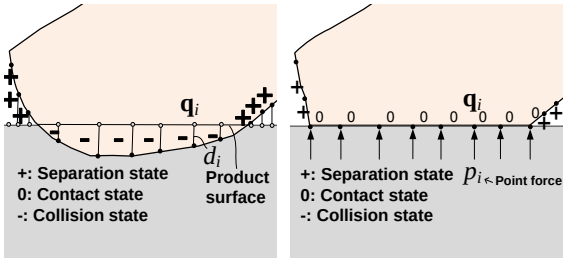

(a) (b)

Figure.9 LCP. (a) Initial situation, (b) Contact situation

Table.1 Computation performance of deformation simulation

	Response matrix	Pre-process	Online process	Hardware
Fingerpad (234 vertices)	1	34s	42 - 80ms	Intel Core i5 1.70GHz, 4GB main memory
Palm (869 vertices)	1	460s	0.26 - 1.98s	
Grasping hand (9693 vertices)	19	19 min	20s	

5. Simulation and Experimental Verifications

5.1 Finger and Palm Deformation

Table 1 shows the performance of our deformation simulation; a real time process can be realized for fingerpad deformation because of the small size of the response matrix. On the contrary, for palm deformation, our simulation took 0.2 to 1.98s depending on the maximum penetration depth.

Figure 10 illustrates the visual effect of deformation simulations of a middle fingerpad (penetration depth: 2.98mm) and a palm (6.10mm). In Fig.10 (b) and (d), the fingerpad and the palm touch the product surfaces without any interpenetration, and obvious bulges resulting from our proposed compressing-swelling effect can be observed.

The experiments were conducted which verified the contact deformation of the fingerpad (subjects: 4 males, 23-26, right middle finger) and palm (subjects: 5 males, 24-51, right hand palm). The experimental settings are

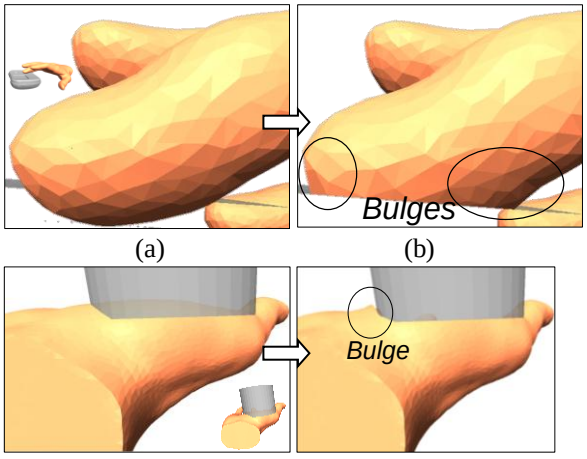

Figure.10 Simulation effect of finger and palm. (a) Before fingertip deformation, (b) After fingertip deformation, bulges can be observed, (c)Before palm deformation, (d) After palm deformation, bulges can be observed.

shown in Fig.11 (a) and Fig.12 (a): a laser ranger (KEYENCE IL-030,) was used to measure the penetration depth; a scale (AND EW-12Ki) was used to measure the contact force; a camera (Logitech HD Pro Webcam C910) was used to measure the contact area. The computer was used for image processing (OpenCV) (Fig.11 (c) and Fig.12 (c)) and for synchronous data acquisition. The fixture made of a foam material was used to support and fix the palms. In the fingerpad measurement, the subjects were asked to press the transparent rigid plate covered by a semi transparent paper using their inked fingerpads. In the palm measurement, a rigid plate covered by a semi transparent paper pressed the inked palms of subjects. At the same time, the measured data was synchronously collected.

Figure 13 shows the relations among maximum depth, contact area (the sum of area of each triangle in the contact region) and contact force (the sum of the point force at each vertex in the contact region) of the fingerpad and palm in the contact deformation. In Fig.13 (a) and (c), the simulation based on the proposed nonlinear elasticity model could effectively agree with the range of measured contact forces of the different subjects compared with the ones using the linear elasticity model with a constant shear modulus. By adjusting the range of varying shear modulus from 5kPa to 120kPa, our simulation could cover all of the experimental data.

Moreover, in Fig.13 (b) and (d), the simulated contact area was within the range of experimental data, and almost overlapped curves were obtained in different shear modulus, because different contact forces resulted in a relatively constant height of swelling bulges (Section.3.5).

5.2 Deformation of Grasping Hand

Simulating grasp posture with hand skin contact deformation is a valuable application of the Digital

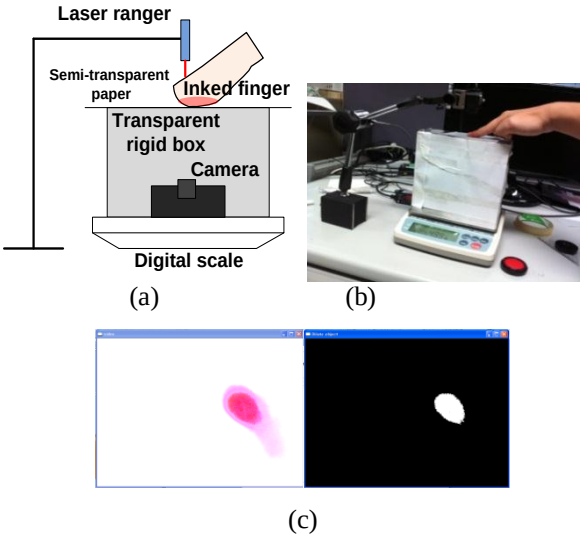

Figure.11 Experiment verifying finger deformation. (a)Experiment setting, (b)Real scene, (c)Image of an contact area before and after the image process

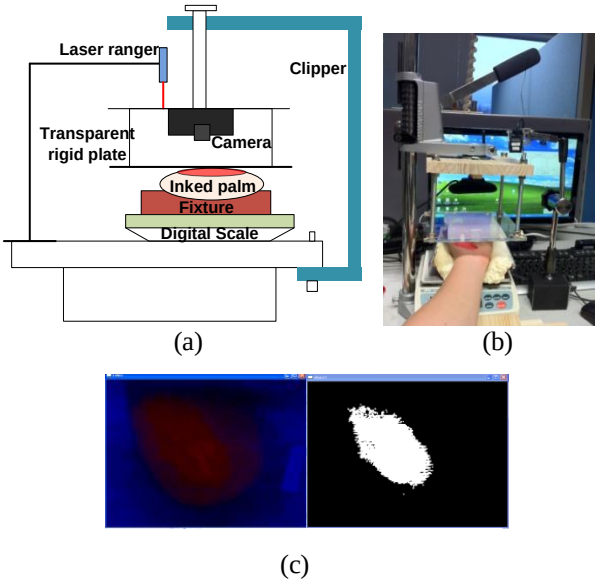

Figure.12 Experiment verifying palm deformation. (a)Experiment setting, (b) Real scene, (c) Image of a contact area before and after the image process

Hand. In order to verify the simulated skin deformation in grasp postures, as shown in Fig.14, a subject (male, 27, right hand) was asked to take an MRI measurement to obtain a hand posture grasping a cylinders whose diameter was ϕ48mm (Fig.14 (a)). As shown in Fig.15, the subject was also asked to take pressure distribution measurements using a sheet type pressure sensor (NITTA FSCAN) with 4.2 sensors/cm^2 (Fig.15 (a)) in the same grasping postures (48mm cylinder grasp) as shown in Fig.14 (b), so that the grasp fits to the handprint marks of the MRI measurements. On the other hand, a Digital Hand model of the same subject was made from the MRI measurements. The grasp posture of the Digital Hand model was reconstructed so that the bone meshes and skin surface mesh of the model fitted with the ones in the cylinder grasp in MRI measurements. As a result, very

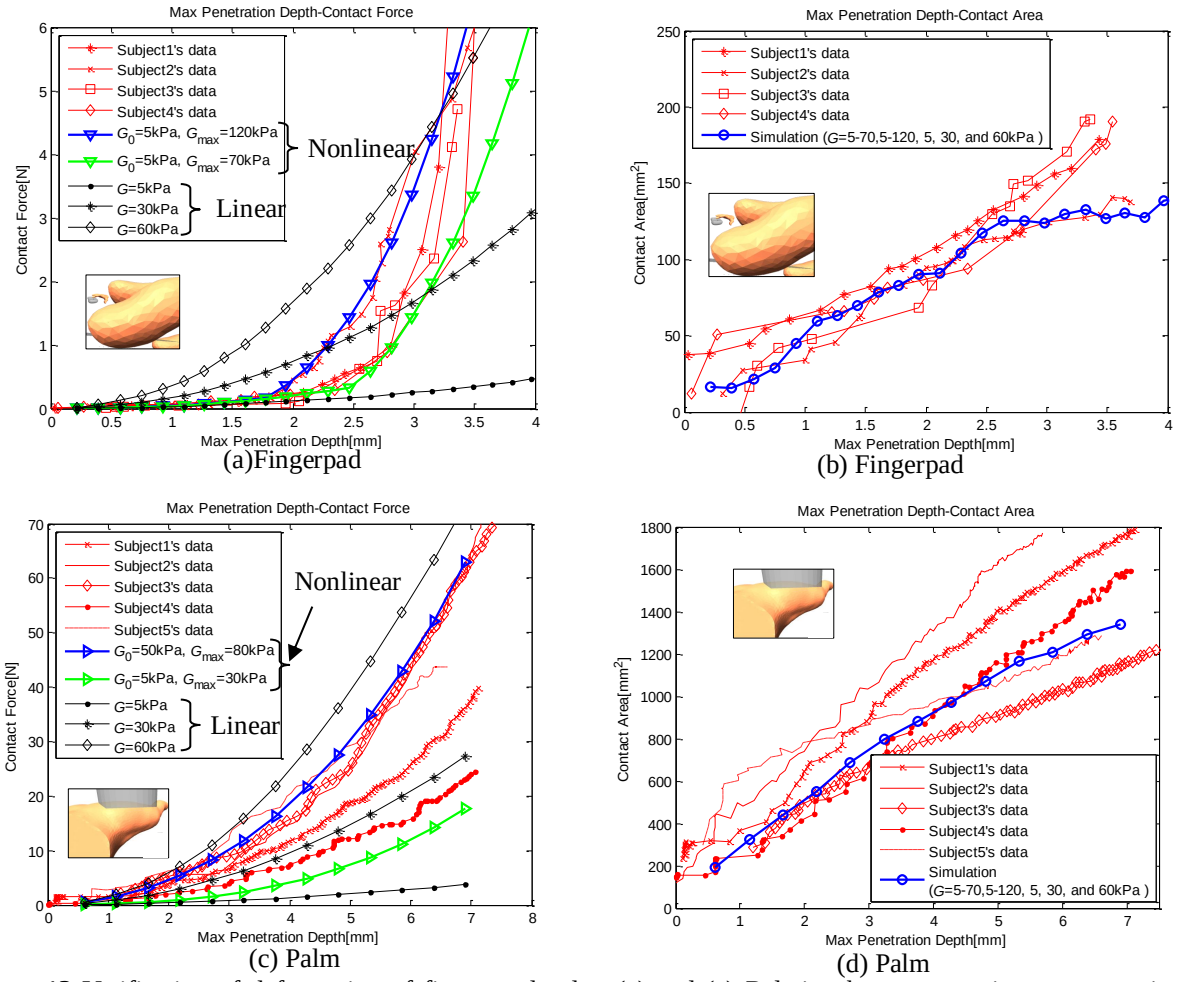

Figure.13 Verification of deformation of finger and palm. (a) and (c) Relation between maximum penetration displacement and contact force (from top to bottom: finger, palm) , (b) and (d) Relation between maximum penetration displacement and contact area (from top to bottom: finger, palm)

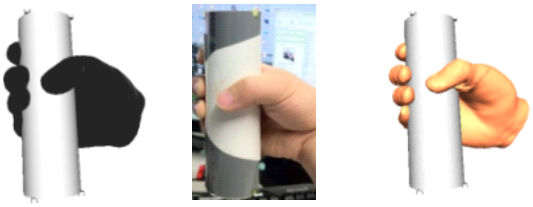

(a) (b) (c)

Figure.14 Similar grasp postures gripping a cylinder of ϕ 48mm. (a) MRI measured grasp posture, (b) Real grasp posture photo, (c) Simulated grasp posture generated by Digital Hand

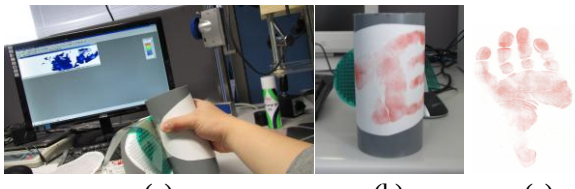

(a) (b) (c)

Figure.15 Experiment verifying pressure distribution of grasp posture. (a) FSCAN system, (b) Sensors mat covered by handprint, (c) Handprint

similar grasp postures (Fig.14 (c)) of the Digital Hand to the experimental ones were generated. Figure 16 shows

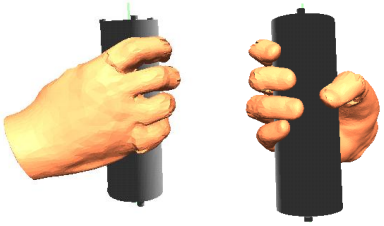

Figure.16 Grasp posture with ϕ 48mm cylinder generated by Digital Hand

the generated grasp posture of the Digital Hand in different views. Figure 17 shows the visual skin deformation effect of the hand in grasp with the ϕ48mm cylinder. Figure 17 (a) shows the hand skin without our contact deformation simulation. In Fig.17 (b), similarly, the Digital Hand touched the cylinder surface with our contact deformation simulation. Figure 17 (c) and (e) shows the simulated pressure distribution map in different views obtained by our model.

From Table.1, 19 response matrices for 19 partitioned regions were pre-computed in about 19 minutes according to the partition of the hand surface shown in Fig.7. The largest size of the matrices was 869 by 869. For the same Digital Hand model, once the response

Table.2 Comparison of pressure distribution between the simulation and the 30s measuement (mean±1SD)

	Cylinder diameter	Spacial peak pressure [MPa]	Spacial average pressure [MPa]	Normal force [N]	Overlapped area [%]
Measurement	ϕ48mm	0.165±0.024	0.033±0.003	337±46	
Simulation		0.170	0.041	313	69%

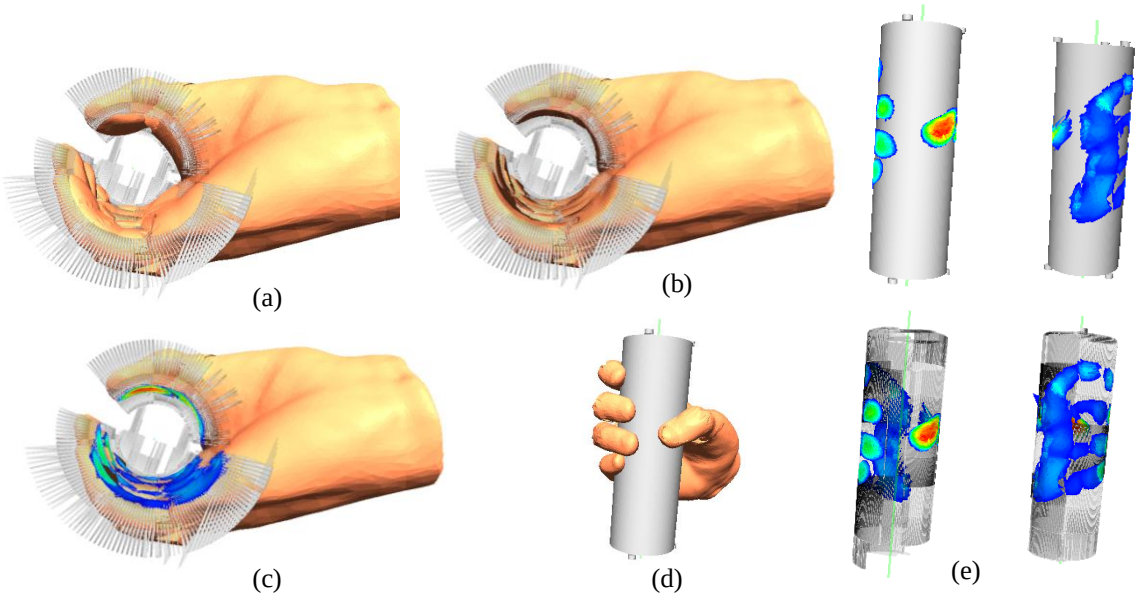

Figure.17 Simulation of grasp posture gripping a ϕ 48mm cylinder. (a) Skin before deformation, (b) Skin after deformation, (c) Estimated pressure distribution map, (d)Grasp posture from another view, (e) Estimated pressure distribution map from various views

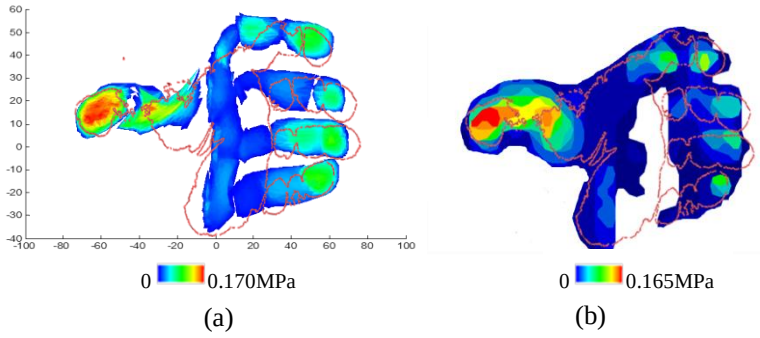

Figure.18 Pressure distribution verification(ϕ 48mm cylinder). Red boundary is contour of the handprint. (a) Simulated pressure distribution, (b) Measured pressure distribution extracted from a 30s measurement

matrices are prepared, they can be reused in generated different grasp postures for the online process. And the online process only took about 20s.

For verifying the simulated pressure distribution, and estimated contact force, contact area, a 30s measurement of pressure distribution was carried out by the pressure sensor. And the time mean among the spacial peak pressures appeared in every frame was extracted. In Fig.18 the extended estimated pressure distribution map from 3D cylinder surfaces (Fig.18 (a)) was compared to the extracted frame (Fig.18 (b)). The entire shape of pressure distribution and the positions of local high pressures between simulation and measurement are very close to each other.

The quantitative comparison results between the simulation and the 30s measurement were summarized in Table.2. Our simulated space peak pressure, space average pressure, and normal force were similar with the measured ones. As for the contact area, their overlaps between simulation and handprints accounted for a larger percentage (69%) of the hand prints.

Of course, there are still some differences among the simulation, the measurement and the handprint as shown in Fig.18. The area showed by handprint, actually, was the accumulated contact area during a 30s measurement. During the measurement, the grasping hand, inevitably

and naturally, slightly quivered, especially in fingertips, therefore, the area of the handprint was larger than the actual instantaneous contact area at a point of time. Moreover, some differences were mainly caused by the following reasons: 1) the bending stresses caused by the warp of the sheet type pressure sensor attached to the cylinder, 2) the biased stresses of sticking the sensor to the cylinder, and 3) the subtle difference between the real grasp posture and the generated one. On the other hand, the current Digital Hand lacks sufficient swelling deformation in the root regions of the fingers caused by finger bending, which led to the missing of the pressure in such regions.

6. Conclusion and Future Work

For the application of hand skin deformation in virtual ergonomic assessment, we have introduced a physical model of nonlinear elasticity and compressing-swelling effect and presented an efficient method simulating contact deformation. The hand surface was partitioned into different regions for efficiency and accuracy. The visual realistic simulation effect was efficiently realized in finger, palm and grasp posture simulation. And the simulation results were experimentally verified. The results showed that the simulations based on our physical model could derive the contact area, the contact force and the contact pressure distribution in the case of the cylinder grasp which was acceptable for virtual ergonomic assessment.

Because the hand skin is a direct medium to sense the objects by physical contact, we believe that constructing a deformable human hand model in contact will be a meaningful application in virtual ergonomic assessment for handheld products, and provide firsthand information for other virtual ergonomic assessment techniques, for instance, and force analysis for maintaining a stable grasp posture, an internal force load acting on finger tendons and muscles.

References

[1] Endo Y, Kanai S, Kishinami T, Miyata N, Kouchi M, Mochimaru M, 2007, Virtual Ergonomic Assessment on Handheld Products based on Virtual Grasping by Digital Hand, SAE 2007 Transactions Journal of Passenger Cars: Electronic and Electrical Systems,Vol.116, No.7, pp.877-887.

[2] Shimizu Y, Kawaguchi K, Kanai S. 2010. Constructing MRI-based 3D Precise Human Hand Models for Product Ergonomic Assessments. In: Proceedings of 2010 Asian Conference on Design and Digital Engineering. Jeju, Korea. pp.837-844.

[3] Dandekar K, Raju BI, Srinivasan MA, 2003, 3-D Finite-Element Models of Human and Monkey Fingertips to Investigate the Mechanics of Tactile Sense, Journal of Biomechanical Engineering, Vol.125, No.5, pp.682-691.

[4] Delalleau A, Josse G, Lagarde JM, Zahouani H, Bergheau JM, 2008, A nonlinear elastic behavior to identify the mechanical parameters of human skin in vivo, Skin Research and Technology, Vol.14, No.2, pp.152-164.

[5] Hall C, 1997, External pressure at the hand during object handling and work with tools, International Journal of Industrial Ergonomics, Vol.20, No.3, pp.191-206.

[6] Aldien Y, Welcome D, Rakheja S, Dong R, Boileau PE, 2005, Contact pressure distribution at hand–handle interface: role of hand forces and handle size, International Journal of Industrial Ergonomics, Vol.35, No.3, pp.267-286.

[7] Seo, N.J., Armstrong, T.J., Ashton-Miller, J., 2006, Grip Forces Measured with Different Methods. In Proceedings of the 16th World Congress on Ergonomics, International Ergonomics Association, Maastricht, Netherlands.

[8] ElKoura G, Singh K. 2003. Handrix: animating the human hand. In: Proceedings of the 2003 ACM SIGGRAPH/Eurographics symposium on Computer animation. San Diego, California: Eurographics Association. pp.110-119.

[9] Sueda S, Kaufman A, Pai DK, 2008, Musculotendon simulation for hand animation, ACM Trans Graph, Vol.27, No.3, pp.1-8.

[10] Rhee T, Neumann U, Lewis JP. 2006. Human hand modeling from surface anatomy. In: Proceedings of the 2006 symposium on Interactive 3D graphics and games. Redwood City, California: ACM. pp.27-34.

[11] Liu CK., 2009, Dextrous manipulation from a grasping pose, ACM Trans Graph, Vol.28, No.3, pp.1-6.

[12] Miyata N, KourchiI M, Mochimaru M, Kawachi K, Kurihara T. 2005. Hand link modeling and motion generation from motion capture data based on 3D joint kinematics. New York, NY, ETATS-UNIS: Society of Automotive Engineers.

[13] Xydas N, Bhagavat M, Kao I. 2000. Study of soft-finger contact mechanics using finite elements analysis and experiments. In: Proceedings of International Conference of Robotics and Automation, 2000. ICRA '00. Vol.2173,pp.2179-2184.

[14] Bickel B, Bacher M, Otaduy MA, Matusik W, Pfister H, Gross M, 2009, Capture and modeling of non-linear heterogeneous soft tissue, ACM Trans Graph, Vol.28, No.3, pp.1-9.

[15] Tao GQ, Li JY, Jiang XF. 2011. Research on virtual testing of hand pressure distribution for handle grasp. In: Mechatronic Science, Electric Engineering and Computer (MEC), 2011 International Conference. Hangzhou, China, pp.1610-1613.

[16] Pauly M, Pai DK, Guibas LJ. 2004. Quasi-rigid objects in contact. In: Proceedings of the 2004 ACM SIGGRAPH/Eurographics symposium on Computer animation. Grenoble, France: Eurographics Association. pp.109-119.

[17] Jain S, Liu CK. 2011. Controlling physics-based characters using soft contacts. In: Proceedings of the 2011 SIGGRAPH Asia Conference. Hong Kong, China: ACM. pp.1-10.

[18] K. L. Johnson, Contact Mechanics, Cambridge Univ. Press, Cambridge, 1985. pp.11-83.
[19] Holzapfel GA, 2000, Biomechanics of soft tissue, Report. pp.1-4.
[20] Srinivasan MA, Gulati RJ, Dandekar K, 1992, In Vivo Compressibility of the Human Fingertip, Advances in Bioengineering, Vol.BED-22, pp.573-576.
[21] Wu JZ, Krajnak K, Welcome DE, Dong RG, 2008, Three-Dimensional Finite Element Simulations of the Dynamic Response of a Fingertip to Vibration, Journal of Biomechanical Engineering, Vol.130, No.5, pp.054501.
[22] Diridollou S, Vabre V, Berson M, Vaillant L, Black D, Lagarde JM, Grégoire JM, Gall Y, Patat F, 2001, Skin ageing: changes of physical properties of human skin in vivo, International Journal of Cosmetic Science, Vol.23, No.6, pp.353-362.
[23] Tenenbaum JB, Silva Vd, Langford JC, 2000, A Global Geometric Framework for Nonlinear Dimensionality Reduction, Science, Vol.290, No.5500, pp.2319-2323.
[24] Murty K. G., Yu FT, 1988, Linear complementarity, linear and nonlinear programming. Sigma Series in Applied Mathematics. 3. Heldermann Verlag, Berlin, pp.85-104.